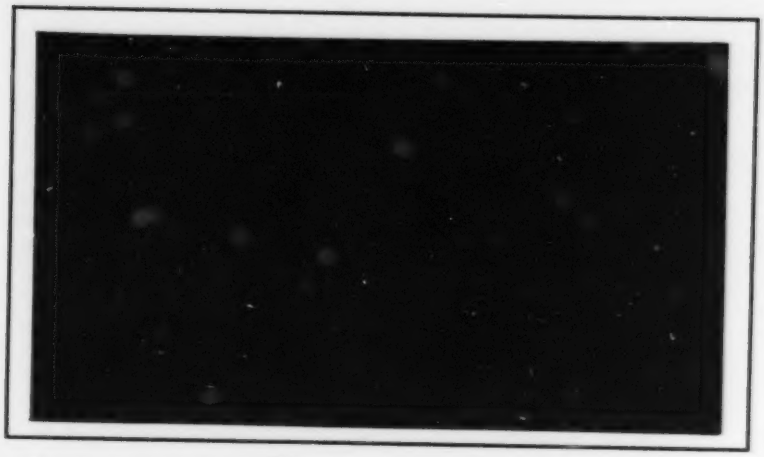

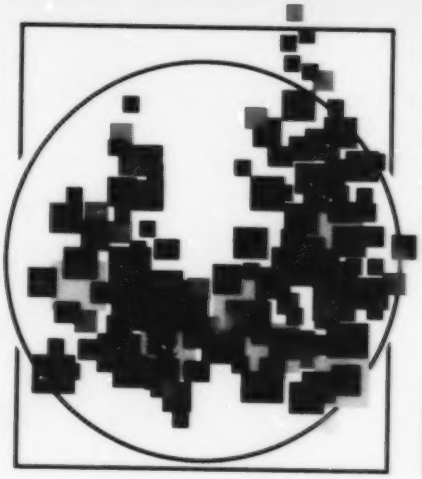

CENTRE FOR
SYSTEMS
SCIENCE

LCCR

Simon Fraser University, Burnaby, B.C., Canada V5A 1S6 / (604) 291-4704

AN ANALYSIS OF PILOT SYMBOL ASSISTED MODULATION FOR RAYLEIGH FADING CHANNELS

James K. Cavers

CSS/LCCR TR 89-16

December 1989

92-05705/

AN ANALYSIS OF PILOT SYMBOL ASSISTED MODULATION FOR RAYLEIGH FADING CHANNELS

by

James K. Cavers

Communications Sciences Laboratory
School of Engineering Science
Simon Fraser University
Burnaby B.C. V5A 1S6
CANADA

(604) 291-3281

ABSTRACT

Proposals have appeared recently for the use of pilot symbols to mitigate the effects of rapid fading in mobile communications. Unlike the more familiar pilot tone systems, pilot symbol assisted modulation (PSAM) does not affect the transmitted pulse shape or the peak-to-average power ratio, and implementation is straightforward. This paper puts PSAM on a solid analytical basis, a feature missing from previous work. It presents closed form expressions for the BER in BPSK and QPSK, for a tight upper bound on SER in 16QAM, and for the optimized receiver coefficients. The error rates obtained are lower than for differential detection for any combination of SNR and doppler spread, and the performance is within 1 dB of a perfect reference system under slow fading conditions, and within 3 dB when the doppler spread is 5% of the symbol rate.

November 1989

This work was funded by the BC Advanced Systems Institute through a Senior Fellowship

ABSTRACT

Proposals have appeared recently for the use of pilot symbols to mitigate the effects of rapid fading in mobile communications. Unlike the more familiar pilot tone systems, pilot symbol assisted modulation (PSAM) does not affect the transmitted pulse shape or the peak-to-average power ratio, and implementation is straightforward. This paper puts PSAM on a solid analytical basis, a feature missing from previous work. It presents closed form expressions for the BER in BPSK and QPSK, for a tight upper bound on SER in 16QAM, and for the optimized receiver coefficients. The error rates obtained are lower than for differential detection for any combination of SNR and doppler spread, and the performance is within 1 dB of a perfect reference system under slow fading conditions, and within 3 dB when the doppler spread is 5% of the symbol rate.

I. INTRODUCTION

Rapid fading is a central problem in digital mobile communications. It degrades the bit error rate (BER), and frquently introduces an irreducible BER, or error floor. It also inhibits the use of multilevel modulation formats, with their greater spectral efficiency.

The use of a pilot tone to mitigate the effects of fading has been explored by several authors [1-4]. The tone provides the receiver with an explicit amplitude and phase reference for detection, and thereby suppresses the error floor. The question of where in the spectrum to locate the tone is a difficult one. Perhaps the best known solution is transparent tone-in-band, or TTIB [1,2,4]. Although it is a general solution, it requires relatively complex signal processing and results in an increased peak-to-average power ratio.

Recently, pilot symbol assisted modulation (PSAM) has been proposed [5,6] as an alternative. The transmitter periodically inserts known symbols, from which the receiver derives its amplitude and phase reference. Like pilot tone modulation, PSAM suppresses the error floor and enables multilevel modulation. However, it does so with no change to the transmitted pulse shape or peak to average power ratio. Processing at the transmitter and receiver is also simpler than with TTIB.

Previous studies of PSAM [5,6] were based on simulation and experimental implementations. Although they demonstrated feasibility, they did not provide the performance analysis needed before their results can be generalized. The present paper supplies the missing analysis. It includes closed form results for the BER in BPSK and QPSK, and for a tight upper bound on the symbol error rate in 16QAM, as well as expressions for the optimum interpolator at the receiver. No numerical integrations are required, though optimization requires solution of the normal equations. The performance of the optimized system is excellent, within 3 dB of an unachievable perfect reference system, even when the doppler spread is 5% of the symbol rate. At 1% doppler, the loss is only 1 dB, and it can be further reduced at lower doppler values.

II. SYSTEM MODEL

A. General Description

A PSAM system can be represented by the block diagram of Figure 1. Known symbols are inserted periodically into the data sequence prior to pulse shaping, and the composite signal is transmitted in the usual way over a channel characterized by flat fading and additive noise. The resulting frame structure is shown in Figure 2. For simplicity, we will assume Rayleigh fading, though the extension to Rice fading is straightforward.

After matched filter detection, the receiver splits the per-symbol samples into two streams. The reference branch decimates the samples to extract those due to the pilot symbols, and interpolates them to form an estimate of the channel state. It then scales and rotates a reference decision grid (shown in Figure 1 for 16QAM) with the estimate, and feeds the modified decision boundaries to the data branch. The data branch contains a delay to compensate for the interpolation delay in the reference branch. As we shall see, this is a more profitable way to view receiver operation than the usual formulation [1-6], in which the receiver normalizes the data branch by dividing it with the estimate from the reference branch.

There are two immediate consequences of the technique. The first is delay in the receiver: in order to obtain enough pilot samples for a good channel estimate, the receiver must wait and buffer samples for several frames. The second is that the interpolation coefficients used to form the channel estimate depend on the position within the frame of the sample whose identity is to be determined.

B. Transmitted Signal

The transmitted signal has a complex envelope given by:

$$s(t) = A \sum_{k=-\infty}^{\infty} b(k)p(t-kT) \qquad (1)$$

where T is the symbol duration, b(k) is the kth symbol value for BPSK, QPSK or a general QAM, A is an amplitude factor, and p(t) is a unit energy pulse:

$$\int_{-\infty}^{\infty} |p(t)|^2 dt = 1 \tag{2}$$

The symbols are formatted into frames of length M in which the pilot symbols at times $i = kM$ have a known value $\tilde{b}$. As noted in [5], it is better to randomize the pilot values to avoid transmitting tones, but this does not affect the analysis.

C. *Fading Channel Effects*

The fading channel output is given by:

$$r_c(t) = c(t)s(t) + n_c(t) \tag{3}$$

in which $n_c(t)$ is AWGN with power spectral density N_o in both real and imaginary components. The channel's complex gain $c(t)$ incorporates both fading and frequency offset:

$$c(t) = \exp(j2\pi f_o t)g(t) \tag{4}$$

where f_o is the residual frequency offset after AFC, and $g(t)$ is the complex Gaussian fading process with variance σ_g^2 and doppler spread f_D. Its autocorrelation function can be written:

$$R_c(\tau) = \sigma_g^2 \tilde{R}_c(\tau) \tag{5}$$

where $\tilde{R}_c(\tau)$ is the unit power equivalent. Although the analysis is not limited to a specific autocorrelation function, in the numerical results presented later, we assume the normalized version to be:

$$\tilde{R}_c(\tau) = \exp(j2\pi f_o \tau)\, J_o(2\pi f_D \tau) \tag{6}$$

which has the U-shaped power spectrum characteristic of isotropic scattering [7].

D. *Receiver Processing*

The receiver detects the pulses using a matched filter with impulse response $p^*(-t)/\sqrt{N_o}$, where the noise normalization is for later notational convenience. We assume no intersymbol interference, which implies Nyquist I pulses with no receiver timing error and fading slow enough not to cause appreciable distortion of the pulses. As a point of

interest, a 5% doppler shift results in only 1% maximum ISI in the case of 25% rolloff spectral raised cosine pulses.

It is convenient at this point to introduce conventional received SNR measures. Define the ratio q of pilot power to data power:

$$q = |\tilde{b}|^2 / (M-1)E[|b|^2] \tag{7}$$

where the expectation is taken over data symbols only. The expected total energy received over a frame is:

$$E_f = \sigma_g^2 A^2 \left(|\tilde{b}|^2 + (M-1)E[|b|^2] \right) \tag{8}$$

With n bits per symbol, and M-1 data symbols in a frame, the received energy per data bit is:

$$E_b = \frac{\sigma_g^2 A^2}{n(M-1)} |\tilde{b}|^2 \left(\frac{1+q}{q} \right) \tag{9}$$

The symbol-spaced samples r(kT) of matched filter output are given by:

$$r(k) = \frac{A\, c(kT)}{\sqrt{N_o}} b(k) + n(k) = u(k)\, b(k) + n(k) \tag{10}$$

where the Gaussian noise samples n(k) are white with unit variance and the symbol gain u(k), as defined here, has variance:

$$\sigma_u^2 = \frac{1}{2} E[|u|^2] = \gamma_b \frac{n(M-1)}{|\tilde{b}|^2} \frac{q}{1+q} \tag{11}$$

in which $\gamma_b = E_b/N_o$.

Without loss of generality, take b(0) be a pilot symbol, and consider the detection of b(k), $-\lfloor M/2 \rfloor \le k \le \lfloor (M-1)/2 \rfloor$. The channel state estimator prepares an estimate of the symbol gain u(k) in (10) using the K nearest pilot samples:

$$v(k) = \sum_{i=-\lfloor K/2 \rfloor}^{\lfloor K/2 \rfloor} h^*(i,k)\, r(iM) \tag{12}$$

Note that the coefficients h(i,k) depend on the position k within the frame. The estimation error is denoted by e(k), so that:

$$u(k) = v(k) + e(k) \tag{13}$$

E. Optimum Interpolation

Previous descriptions of PSAM used plausible, but arbitrary, interpolation filters: a lowpass in [5] and an approximately Gaussian filter in [6]. Here we use a Wiener filter to minimize the variance of the estimation error e, in order to discover the limits of the technique.

Define the length K column vector $\mathbf{r}$ as the set of pilot samples $r(iM)$, $-\lfloor K/2 \rfloor \le i \le \lfloor K/2 \rfloor$ and $\mathbf{h}(k)$ as the corresponding set of coefficients for the kth position in the frame. Then the estimated symbol gain is given by:

$$v(k) = \mathbf{h}^{\dagger}(k)\mathbf{r} \tag{14}$$

where † denotes conjugate transpose, and the interpolation error is given by:

$$e(k) = u(k) - \mathbf{h}^{\dagger}(k)\mathbf{r} \tag{15}$$

The K x K autocorrelation matrix is:

$$\mathbf{R} = \frac{1}{2} E\left[\mathbf{r}\mathbf{r}^{\dagger} \right] \tag{16}$$

and the M-1 length K covariance vectors are:

$$\mathbf{w}(k) = \frac{1}{2} E\left[u^{*}(k)\mathbf{r} \right] \tag{17}$$

Then the variances of interest are given by:

$$\sigma_v^2(k) = \mathbf{h}^{\dagger}(k)\mathbf{R}\mathbf{h}(k)$$

$$\sigma_{uv}^2(k) = \mathbf{w}^{\dagger}\mathbf{h}(k)$$

$$\sigma_e^2(k) = \sigma_u^2 - 2\mathrm{Re}[\sigma_{uv}^2(k)] + \sigma_v^2(k) \tag{18}$$

As is well known [e.g. 8], an optimum estimate results if the coefficient vector $\mathbf{h}$ is selected to satisfy the normal equations:

$$\mathbf{R}\mathbf{h}(k) = \mathbf{w}(k) \tag{19}$$

The estimation error variance then attains its minimum value, and we

have:

$$\sigma_v^2(k) = \sigma_{uv}^2(k) = \mathbf{w}^\dagger(k)\mathbf{R}^{-1}\mathbf{w}(k)$$

$$\sigma_e^2(k) = \sigma_u^2 - \sigma_v^2 \tag{20}$$

Moreover, the estimation error is uncorrelated with r(iM) and v(k).

In the case at hand, we have explicit expressions for components of the arrays **R** and **w**(k). From (10), (11) and (16), we have:

$$R_{ik} = \gamma_b\, n(M-1)\, \frac{q}{1+q}\, \tilde{R}_c((i-k)MT) + \delta_{ik} \tag{21}$$

where δ_{ik} is the Kronecker delta, and from (7), (10), (11) and (17) we have:

$$w_i(k) = \gamma_b\, \frac{n(M-1)}{\tilde{b}^*}\, \frac{q}{1+q}\, \tilde{R}_c((iM-k)T) \tag{22}$$

Calculation of the optimum interpolation coefficients and the resulting variances is straightforward.

III. BPSK AND QPSK SIGNALLING

A. *Calculation of BER*

First, consider BPSK. The pilot symbols have the value $\tilde{b} = 1$, and the data symbols are $b(k) = \pm 1$. The receiver makes decisions by phase correcting the matched filter output with the channel estimate and comparing the result to zero:

$$\mathrm{Re}[r(k)v^*(k)] \;:\; 0 \qquad \text{(BPSK)} \tag{23}$$

If the transmitted bit is +1, then an error is made if the real part of the decision variable above is negative. Since $r(k)$ and $v(k)$ are correlated, zero mean, Gaussian random variables, we can use a standard result for the probability of this event [8, App 4B]:

$$P_b(k) = \frac{1}{2}\left(1 - \sqrt{\mathrm{Re}[\rho(k)]^2/\left(1 - \mathrm{Im}[\rho(k)]^2\right)}\right) \tag{24}$$

where $\rho(k)$ is the correlation coefficient:

$$\rho(k) = \sigma^2_{rv}(k)/\sigma_r\sigma_v(k) \tag{25}$$

Since $b(k) = 1$, we have $\sigma^2_{rv}(k) = \sigma^2_{uv}(k)$ and $\sigma^2_r = \sigma^2_u + 1$. For an arbitrarily selected filter $\mathbf{h}(k)$, therefore, the correlation coefficient is given by:

$$\rho(k) = \frac{\mathbf{w}^\dagger(k)\mathbf{h}(k)}{\sqrt{(\sigma^2_u + 1)\;\mathbf{h}^\dagger(k)\mathbf{R}\mathbf{h}(k)}} \qquad \text{(BPSK, arbitrary } \mathbf{h}(k)\text{)} \tag{26}$$

where σ^2_u is given by (11). In the case of the optimum filter (19), the correlation coefficient is real:

$$\rho(k) = \frac{\mathbf{w}^\dagger(k)\mathbf{R}^{-1}\mathbf{w}(k)}{\sqrt{(\sigma^2_u + 1)\;\mathbf{w}^\dagger(k)\mathbf{R}^{-1}\mathbf{w}(k)}} \qquad \text{(BPSK, optimum } \mathbf{h}(k)\text{)} \tag{27}$$

and the error probability becomes:

$$P_b(k) = (1-\rho(k))/2 \qquad \text{(BPSK, optimum } \mathbf{h}(k)\text{)} \tag{28}$$

Next, consider QPSK, in which the data symbols are $b(k) = \pm 1 \pm j$. Although the pilot symbol would be selected from this set in practice,

the resulting $\pi/4$ rotation in $v(k)$ must be corrected before use. To simplify the notation, therefore, we will consider the pilot symbols to be real, with the value $\tilde{b} = \sqrt{2}$. The decision criteria are then:

$$\mathrm{Re}[r(k)v^*(k)] \gtrless 0, \quad \mathrm{Im}[r(k)v^*(k)] \gtrless 0 \qquad \text{(QPSK)} \tag{29}$$

We will evaluate the BER for the real component only, since it is the same for the imaginary component. However, if σ_{uv}^2 is complex, the resulting phase bias means we have to average the error probabilities for the two cases $b(k) = \pm 1 + j$, since they differ.

The BER calculation is much like that for BPSK, with the change that $\sigma_{rv}^2 = \sigma_{uv}^2\, b(k)$, so that from (18):

$$\rho(k) = \frac{\mathbf{w}^\dagger(k)\mathbf{h}(k)\; b(k)}{\sqrt{(2\sigma_u^2 + 1)\; \mathbf{h}^\dagger(k)\mathbf{R}\mathbf{h}(k)}} \qquad \text{(QPSK, arbitrary } \mathbf{h}(k)\text{)} \tag{30}$$

with a similar change for optimum $\mathbf{h}(k)$ (30). Note that the definition of $\mathbf{w}(k)$ (17) makes its value, and that of $\mathbf{h}(k)$, different from the BPSK case. Finally, the BER is given by (24), since $\rho(k)$ is complex.

A similar analysis can be applied to M-PSK systems with more than 4 phases [8, App 7A]. Again, the performance is determined by a correlation coefficient.

B. Effect of Interpolation Position

The position of a symbol within the frame determines the estimation error, and hence the BER. Numerical experimentation, though, showed a small position dependence, observable only at very high SNR, where AWGN did not mask the effect. For example, for K=7, in an M=10 symbol frame, with $f_D T = 0.01$ and $\gamma_b = 50$ dB, there was only a 0.8% variation in BER across the frame. For a very short filter (K = 3), fast fading ($f_D T = 0.05$) and 50 dB SNR we found a factor of 3 variation across a 5 symbol frame. However, for normal operating parameters and K greater than 7, we determined that position dependence is negligible. Subsequent sections evaluate the BER only for k = 1, that is, for the symbol immediately following the pilot.

C. *Effect of Pilot Symbol Spacing*

The frame size, or pilot spacing, M has an optimum value, which represents a tradeoff between wasting energy in unnecessary pilot symbols and not sampling the fading process often enough for good estimation. Figure 3 illustrates the effect for BPSK at γ_b = 30 dB, with a variety of fade rates, and a 63 coefficient filter optimized at every point on the graph. Not surprisingly, the BER rises steeply when the frame size causes sampling to fall below the Nyquist rate, i.e. when $M < 1/2f_DT$.

We selected a frame of M = 7 symbols as the benchmark for the rest of the paper; although it represents a 14% loss of capacity, it does accomodate fade rates up to 5% of the symbol rate. If slower fade rates are expected - for example, 100 Hz doppler in a 16 ksymbol/s system gives $f_DT = 6.25 \times 10^{-3}$ - then much larger frames should be adopted, to reduce the loss of capacity.

The loss of capacity is somewhat less than in TTIB [1], a well known pilot tone technique. TTIB requires a bandwidth increase of $2f_D$ for the tone, plus an overlap region of comparable size for synchronization, for a total of about $4f_D$. With symbol spacing T, this is a fractional increase in bandwidth of about $4f_DT$. In comparison, as we saw above, PSAM requires a fractional increase of 1/M, or about $2f_DT$.

As noted earlier, there is some startup delay in PSAM. The receiver must discard several data symbols at the start of each transmission, until it has accumulated enough pilot symbols for useful interpolation. There are about KM/2 such wasted data symbols - about 39 for the values M = 7 and K = 11 we have adopted as a banchmark. This nevertheless compares favourably with TTIB, which has been shown previously [9] to require on the order of 150 symbols to acquire phase lock at the start of a transmission.

D. *Effect of Interpolator Size*

The number of interpolator coefficients is a significant issue, as it affects delay and computational load, as well as BER. Figure 4 shows the dependence on K for BPSK and a 7 symbol frame. Again, the coefficients are optimized at every point. The improvement beyond 5 or

10 coefficients is very slight. In the remaining sections, we use K = 11, though a reduction even to 5 coefficients would not cause serious harm.

E. Performance With Optimized Coefficients

Figure 5 shows BER curves for PSAM BPSK with a 7 symbol frame and 11 coefficient interpolation. The coefficients are optimized at every point. We see that for 0 Hz doppler, PSAM is only 1 dB poorer than the unachievable coherent BPSK. Of the loss, 0.7 dB is attributable to the pilot symbols themselves, which are unnecessarily frequent for $f_D T = 0$, and the remainder is due to the limit of 11 coefficients in the interpolation. Even at 5% doppler, the loss compared with coherent BPSK is only 3.5 dB and, as hoped, there is no error floor, at least in the useful range.

Comparison with DPSK, as calculated from expressions given in [8], shows that PSAM is better than DPSK at all values of SNR and doppler spread. DPSK, of course, develops a significant error floor at large values of doppler.

Comparison with the pilot tone based TTIB is also interesting. It has been shown previously [9] that the phase lock required by TTIB when used for data forces differential encoding, and hence a performance penalty of 3 dB. In contrast, PSAM produces an absolute phase reference, and therefore does not need differential encoding.

The frequency offset f_o has no effect on PSAM BER. By assumption, $f_o T$ and $f_D T$ are both small enough not to introduce intersymbol interference by distorting the pulses, and the optimized coefficients simply introduce compensating phase shifts.

The performance of QPSK has not been illustrated. Its BER is within 2% of that of BPSK for error rates of 10^{-2} or less, as both numerical evaluation and series expansions demonstrate.

F. Effect of Mismatch

The results of Section 3E above are somewhat unrealistic, in that the interpolator coefficients are optimum at every point on the graph. In practice, we would either design an adaptive interpolator or, more

likely, optimize for one operating point, and use those coefficients even if conditions change.

Figure 6 illustrates one such trial, in which the coefficients are optimized for γ_b = 20 dB, 5% doppler, and no frequency offset. The result is that lower values of doppler give no improvement in performance over most of the useful range. Even frequency offset, acting alone, had a negligible effect. However, there is a clear warning in the curve for combined 5% doppler and 1% frequency offset. The very substantial error floor means that AFC must be extremely accurate in the presence of significant doppler spread.

The reappearance of the error floor is readily explained: the frequency offset introduces a phase shift between the estimated and the true channel gain. Since they are no longer perfectly correlated, there is a nonzero probability of error, especially during deep fades.

IV. 16QAM SIGNALLING

A. *Calculation of SER*

In 16QAM we use symbols in which both real and imaginary parts of b(k) take on the values -3, -1, 1, 3, and the expected value $E[|b|^2] = 10$. In the absence of fading, we would use the following six decision boundaries: $Re[r(k)] = 0$, $Im[r(k)] = 0$, $Re[r(k)\pm 2] = 0$, and $Im[r(k)\pm 2j] = 0$. As shown in Figure 7, however, fading scales and rotates the signal constellation. The receiver compensates by scaling and rotating the decision boundaries, using the channel estimate v(k). The six decision boundaries become:

$$\begin{aligned} &Re[rv^*] = 0 \qquad && Re[-jrv^*] = 0 \\ &Re[(r\pm 2v)v^*] = 0 \qquad && Re[(-jr\pm 2v)v^*] = 0 \end{aligned} \tag{31}$$

where we have replaced $Im[\circ]$ with $Re[-j\circ]$ for simplicity, and have dropped the dependence on k, since we determined it to be weak in Section 3B.

A symbol error occurs if r falls outside the decision cell determined by the appropriate boundaries. The probability of this event depends on the transmitted symbol; clearly, it is greater for an interior cell than it is for a corner cell, which has only two boundaries. There are four distinct cell types, for which representative symbols are: $b_1 = 1+j$ (interior cell); $b_2 = 1+j3$ (edge cell); $b_3 = 3+j$ (another edge cell); and $b_4 = 3+j3$ (corner cell). We shall carry the calculations through only for the interior cell with symbol b_1. Calculations for the rest are similar, and are summarized in Appendix A for completeness.

For the given interior cell, an error occurs if any of the following are true:

$$\begin{aligned} &Re[y_{11}v^*] = Re[rv^*] < 0 \\ &Re[y_{12}v^*] = Re[-jrv^*] < 0 \\ &Re[y_{13}v^*] = Re[(2v-r)v^*] < 0 \\ &Re[y_{14}v^*] = Re[(2v+jr)v^*] < 0 \end{aligned} \tag{32}$$

where y_{11} to y_{14}, as defined here, are zero mean Gaussian variates, correlated with v. The probability of each event can therefore be

calculated as in Section 3A:

$$P_e(\rho_{1m}) \approx \frac{1}{2}\left(1 - \sqrt{\mathrm{Re}[\rho_{1m}]^2/(1 - \mathrm{Im}[\rho_{1m}]^2)}\right) \tag{33}$$

where ρ_{1m} is the correlation coefficient relating y_{1m} and v. From the definitions of y_{1m} (32) and r (10), the four correlation coefficients are easily determined to be:

$$\begin{aligned}
\rho_{11} &= b_1\sigma_{uv}^2\left((|b_1|^2\sigma_u^2 + 1)\,\sigma_v^2\right)^{-1/2} \\
\rho_{12} &= -j\rho_{11} \\
\rho_{13} &= \left(2\sigma_v^2 - b_1\sigma_{uv}^2\right)\left((4\sigma_v^2 - 4\mathrm{Re}[b_1\sigma_{uv}^2] + |b_1|^2\sigma_u^2 + 1)\,\sigma_v^2\right)^{-1/2} \\
\rho_{14} &= \left(2\sigma_v^2 + jb_1\sigma_{uv}^2\right)\left((4\sigma_v^2 - 4\mathrm{Im}[b_1\sigma_{uv}^2] + |b_1|^2\sigma_u^2 + 1)\,\sigma_v^2\right)^{-1/2}
\end{aligned} \tag{34}$$

where the variances σ_u^2, σ_{uv}^2 and σ_v^2 are given by (11) and (18). The union bound gives a close approximation to the error rate for symbol b_1:

$$P_{s1} \le \sum_{m=1}^{4} P_e(\rho_{1m}) \tag{35}$$

In practice, the bound is almost indistinguishable from the true value if the SER is below about 0.01, and is useful - within about 10% of the true value - for SER as high as 0.4.

As noted above, a similar calculation must be performed for the other three cell types. Since the four cell types are equally represented, the final calculation for SER is just:

$$P_s = \frac{1}{4}\sum_{i=1}^{4} P_{si} \tag{36}$$

B. Higher Order Constellations

For larger constellations like 64QAM, calculations like those above become very tedious, and upper bounding the overall SER with that of a single interior cell becomes attractive. However, not all interior cells have the same error rate, as can be seen readily from (13). We

can write:

$$r = bv + be + n$$

so that the additive disturbance has variance $|b|^2\sigma_e^2 + 1$. Therefore the cells farthest from the origin - the interior corners - have the highest error rate, and provide the upper bound.

C. Frame Size and Interpolator Size

Figures 8 and 9 illustrate the effect of frame size M and number K of interpolator coefficients for 16QAM. The pilot symbols were selected as the corner symbols $b_4 = 3+j3$; more precisely, they were real symbols of the same magnitude $\sqrt{18}$. It can be seen that M = 7 and K = 11 is a reasonable choice for the baseline system, just as it was for BPSK/QPSK in Section 3.

D. 16QAM With Optimized Coefficients

Figure 10 shows the SER of PSAM with coefficients optimized at every point. For comparison, the lowest curve represents the performance of an ideal system, with perfect phase and amplitude reference, and was obtained by letting M approach infinity in σ_u^2, then setting σ_v^2 and σ_{uv}^2 equal to σ_u^2 before evaluating (34-36). PSAM is about 0.9 dB worse than the ideal system at zero doppler, and only about 2.4 dB worse than ideal at 5% doppler.

In comparing 16QAM with BPSK (Figure 5), note that the 16QAM SER should be divided by 4 to obtain the equivalent BER of a Gray coded constellation. Thus the performance penalty of 16QAM is 3 dB in comparing ideal reference systems, and about 2.1 dB in comparing 16QAM to BPSK at 5% doppler.

Also shown on Figure 10 as SS PSAM is the performance of a system using the 3-point interpolator coefficients specified in [6], calculated with the method of Section 4A after substituting those coefficients in (18). The frame size is 7. For zero doppler, the performance is slightly worse than that of the optimized coefficients at 5% doppler. At 1% doppler, the performance is unacceptable. It is worth noting that these coefficients produce a strong dependence of SER on position within the frame: about 33% at zero doppler, and over an order of magnitude at

1% doppler. The comparison demonstrates the value of both the optimization and the use of a longer interpolator.

E. 16QAM With Mismatched Coefficients

As noted in Section 3F, the operating point of a system could well differ from that for which the coefficients are optimized. Figure 11 shows the performance of a system in which the optimization point is γ_b = 30 dB, f_oT = 0, f_DT = 0.05. The general behaviour is like that in Figure 6, for BPSK: the SER is unaffected by frequency offset and doppler spread, acting individually, up to 5%, but the combination of offset and doppler introduces a significant error floor.

V. CONCLUSIONS

Pilot symbol assisted modulation (PSAM) is relatively simple to implement. The transmitter just inserts known symbols periodically, so there is no change in pulse shape or peak to average power ratio. The receiver interpolates the channel measurements provided by the pilot symbols to obtain an amplitude and phase reference for detection. The pilot symbols lower the effective bit rate by about 14% if the doppler spread is 5% of the symbol rate. For smaller doppler values, though, the loss of capacity is much less: about 5% for a 1% doppler spread. Minor drawbacks include the delay and buffer space required at the receiver for interpolation. However, the good error performance, the removal of the error floor, and the enabling of multilevel signal formats outweigh these deficiencies.

PSAM is straighforward to analyze. We obtained analytical expressions for BER in BPSK and QPSK, for a tight upper bound on SER in 16QAM, and for the optimum interpolation coefficients. For BPSK and QPSK, optimized PSAM's loss compared with the unachievable coherent detection is only 1 dB for very slow fading, and 3 dB for 5% doppler. There is no error floor, as there is in differential detection. Moreover, optimized PSAM outperforms differential detection at any values of doppler and SNR.

Comparison with TTIB is also favourable. PSAM is less complex at both the transmitter and receiver, and does not introduce envelope fluctuations. The loss of capacity, or bandwidth, is somewhat lower in PSAM, and the header preceding each transmission can be much shorter than in TTIB. In addition PSAMdoes not suffer the 3 dB performance penalty incurred by TTIB due to its requirement for differential encoding. However, PSAM does not have the generality of TTIB, which also supports analog transmission.

For 16QAM, optimized PSAM is 0.9 dB poorer in very slow fading than the unachievable system with perfect phase and amplitude reference, and is 2.4 dB poorer at 5% doppler. A comparison PSAM system using previously published interpolation coefficients [6] has poorer performance in very slow fading than optimized PSAM at 5% doppler, and

has a large irreducible error rate at 1% doppler.

Residual frequency offset, after AFC, is a potential problem. Although PSAM with optimized coefficients is insensitive to frequency offset, even in conjunction with doppler spread, the same is not true with other coefficients. For example, PSAM with fixed coefficients optimized for 5% doppler and zero offset is insensitive to doppler and offset values up to 5%, acting individually; however, a combination of doppler and offset results in a significant error floor. The remedy lies in better AFC or in adaptive coefficients.

APPENDIX A

SUMMARY OF CORRELATION COEFFICIENTS FOR 16QAM

For the reader's convenience, we have listed below the correlation coefficients of the four distinct cell types, for which representative symbols are: $b_1 = 1+j$ (interior cell); $b_2 = 1+j3$ (edge cell); $b_3 = 3+j$ (another edge cell); and $b_4 = 3+j3$ (corner cell).

$$\rho_{11} = b_1\sigma_{uv}^2 \left((|b_1|^2\sigma_u^2 + 1)\ \sigma_v^2\right)^{-1/2}$$

$$\rho_{12} = -jb_1\sigma_{uv}^2 \left((|b_1|^2\sigma_u^2 + 1)\ \sigma_v^2\right)^{-1/2}$$

$$\rho_{13} = \left(2\sigma_v^2 - b_1\sigma_{uv}^2\right) \left((4\sigma_v^2 - 4\mathrm{Re}[b_1\sigma_{uv}^2] + |b_1|^2\sigma_u^2 + 1)\ \sigma_v^2\right)^{-1/2}$$

$$\rho_{14} = \left(2\sigma_v^2 + jb_1\sigma_{uv}^2\right) \left((4\sigma_v^2 - 4\mathrm{Im}[b_1\sigma_{uv}^2] + |b_1|^2\sigma_u^2 + 1)\ \sigma_v^2\right)^{-1/2}$$

$$\rho_{21} = b_1\sigma_{uv}^2 \left((|b_2|^2\sigma_u^2 + 1)\ \sigma_v^2\right)^{-1/2}$$

$$\rho_{23} = \left(2\sigma_v^2 - b_2\sigma_{uv}^2\right) \left((4\sigma_v^2 - 4\mathrm{Re}[b_2\sigma_{uv}^2] + |b_2|^2\sigma_u^2 + 1)\ \sigma_v^2\right)^{-1/2}$$

$$\rho_{22} = \left(-2\sigma_v^2 - jb_2\sigma_{uv}^2\right) \left((4\sigma_v^2 - 4\mathrm{Im}[b_2\sigma_{uv}^2] + |b_2|^2\sigma_u^2 + 1)\ \sigma_v^2\right)^{-1/2}$$

$$\rho_{31} = -jb_3\sigma_{uv}^2 \left((|b_3|^2\sigma_u^2 + 1)\ \sigma_v^2\right)^{-1/2}$$

$$\rho_{32} = \left(-2\sigma_v^2 + b_3\sigma_{uv}^2\right) \left((4\sigma_v^2 - 4\mathrm{Re}[b_3\sigma_{uv}^2] + |b_3|^2\sigma_u^2 + 1)\ \sigma_v^2\right)^{-1/2}$$

$$\rho_{33} = \left(2\sigma_v^2 + jb_3\sigma_{uv}^2\right) \left((4\sigma_v^2 - 4\mathrm{Im}[b_3\sigma_{uv}^2] + |b_3|^2\sigma_u^2 + 1)\ \sigma_v^2\right)^{-1/2}$$

$$\rho_{41} = \left(-2\sigma_v^2 + b_4\sigma_{uv}^2\right) \left((4\sigma_v^2 - 4\mathrm{Re}[b_4\sigma_{uv}^2] + |b_4|^2\sigma_u^2 + 1)\ \sigma_v^2\right)^{-1/2}$$

$$\rho_{42} = \left(-2\sigma_v^2 - jb_4\sigma_{uv}^2\right) \left((4\sigma_v^2 - 4\mathrm{Im}[b_4\sigma_{uv}^2] + |b_4|^2\sigma_u^2 + 1)\ \sigma_v^2\right)^{-1/2}$$

where the variances σ_u^2, σ_v^2 and σ_{uv}^2 are given in (11) and (18).

REFERENCES

[1] J.P. McGeehan and A.J. Bateman, "Phase Locked Transparent Tone-in-Band (TTIB): A New Spectrum Configuration Particularly Suited to the Transmission of Data Over SSB Mobile Radio Networks", IEEE Trans Commun, vol COM-32, no 1, pp 81-87, January 1984.

[2] A.J. Bateman et al, "Speech and Data Communications Over 942 MHz TAB and TTIB Single Sideband Mobile Radio Systems Incorporating Feed-Forward Signal Regeneration", IEEE Trans Vehicular Techn, vol vt-34, no 1, pp 13-21, February 1985.

[3] F. Davarian, "Mobile Digital Communications via Tone Calibration", IEEE Trans Vehicular Techn, vol VT-36, pp 55-62, May 1987.

[4] P.M. Martin et al, "The Implementation of a 16-QAM Mobile Data System Using TTIB-Based Fading Correction Techniques", Proc IEEE Vehicular Techn Conf, pp 71-76, Philadelphia, 1988.

[5] M.L. Moher and J.H. Lodge, "TCMP - A Modulation and Coding Strategy for Rician Fading Channels", IEEE J. Selected Areas in Communications, 1990.

[6] S. Sampei and T. Sunaga, "Rayleigh Fading Compensation Method for 16QAM in Digital Land Mobile Radio Channels", Proc IEEE Vehicular Techn Conf, pp 640-646, San Francisco, May 1989.

[7] W.C.Y. Lee, Mobile Communications Engineering, McGraw-Hill, 1982.

[8] J.G. Proakis, Digital Communications, McGraw-Hill, 1983.

[9] J.K. Cavers, "Phase Locked Transparent Tone-in- Band: An Analysis", Proc IEEE Vehicular Techn Conf, pp73-77, San Francisco, May 1989.

ILLUSTRATIONS

Figure 1: Organization of a Pilot Symbol System

Figure 2: Transmitted Frame Structure

Figure 3: Effect of Frame Size on BPSK (γ_b=30 dB, K=63)

Figure 4: Effect of Interpolator Size on BPSK (M=7)

Figure 5: BER Performance of Optimized PSAM for BPSK

Figure 6: PSAM BPSK: Mismatched With Coefficients Optimized for γ_b=20 dB, f_oT=0, f_DT=0.05

Figure 7: 16QAM Constellation and Decision Boundaries in Fading

Figure 8: Effect of Frame Size on 16QAM (γ_b=30 dB, K=63)

Figure 9: Effect of Interpolator Size on 16QAM (M=7)

Figure 10: SER Performance of Optimized PSAM for 16QAM

Figure 11: PSAM 16QAM: Mismatched With Coefficients Optimized for γ_b=30 dB, f_oT=0, f_DT=0.05

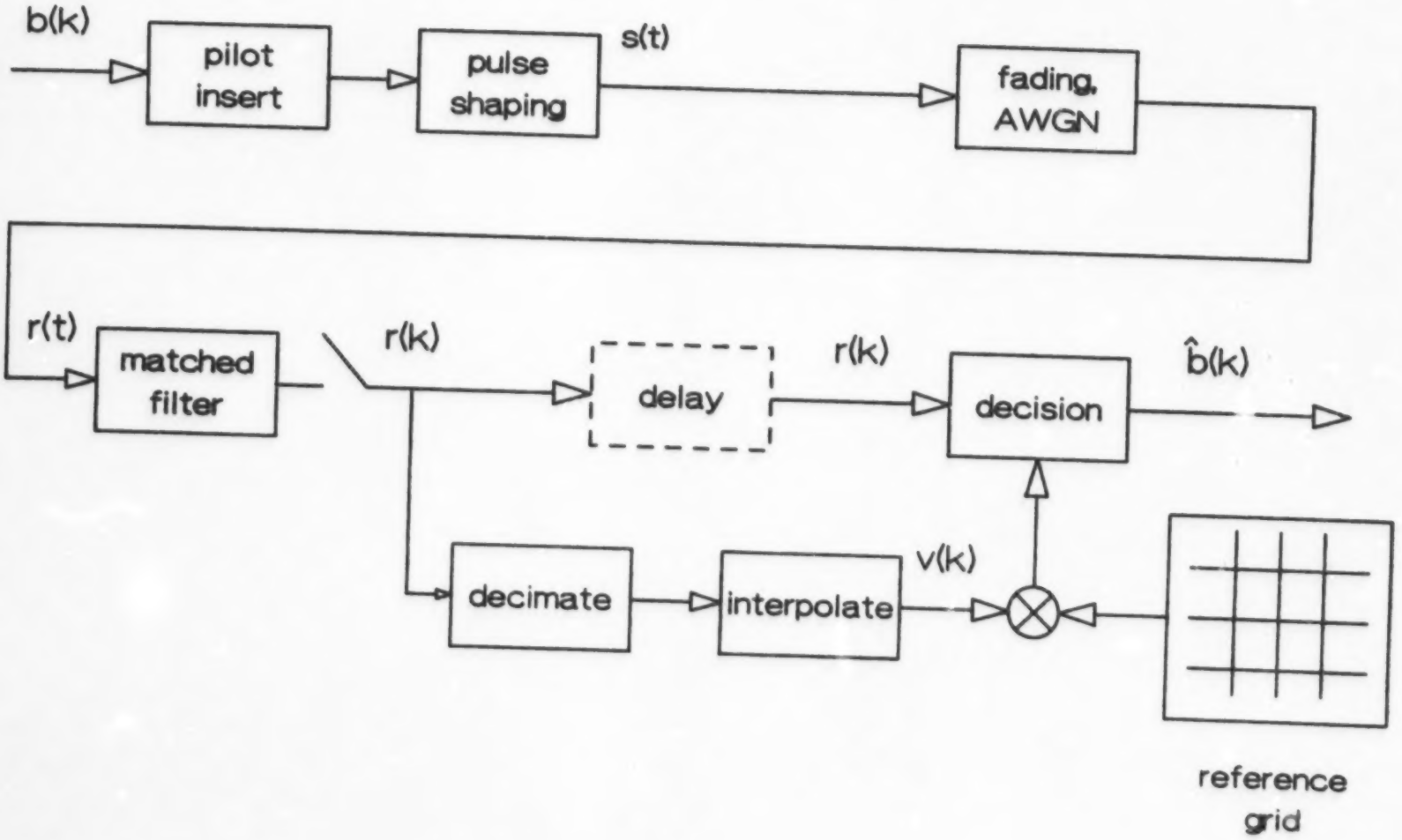

Figure 1: Organization of a Pilot Symbol System

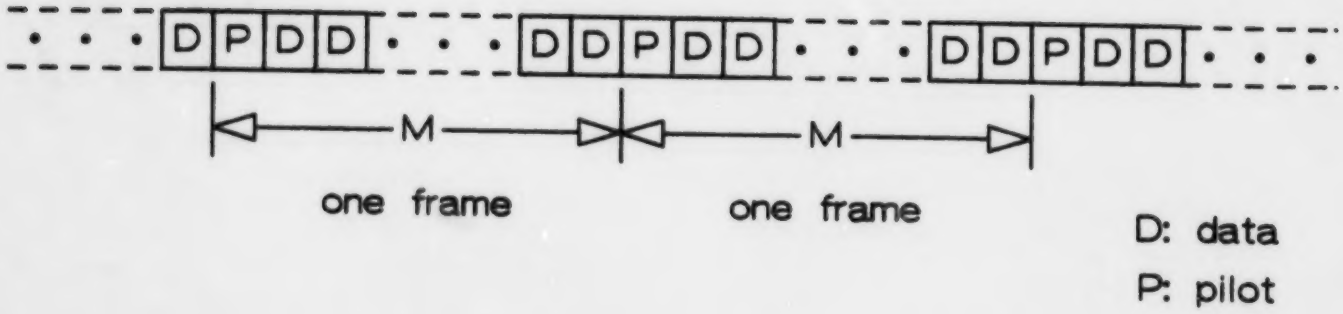

Figure 2: Transmitted Frame Structure

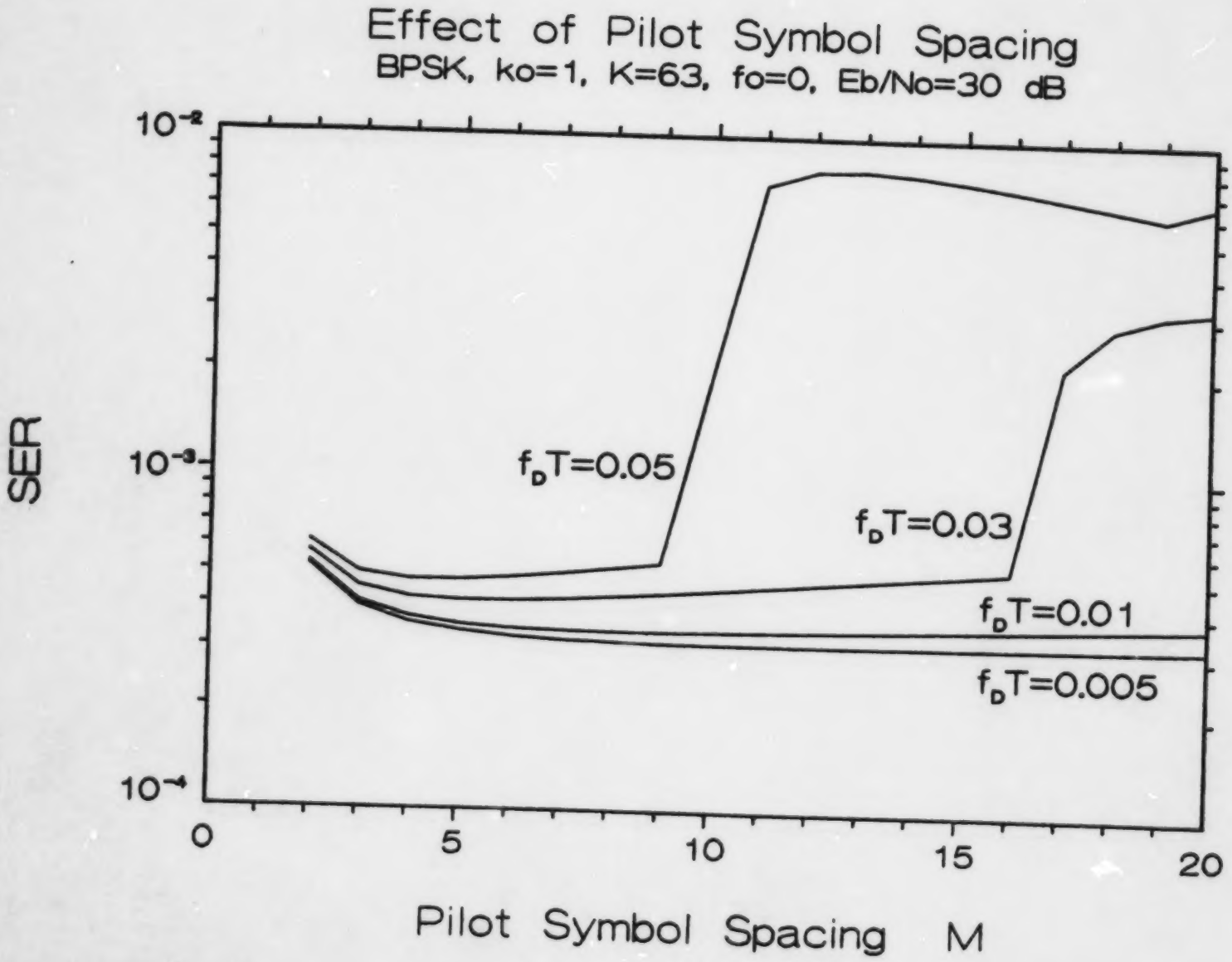

Figure 3: Effect of Frame Size on BPSK (γ_b=30 dB, K=63)

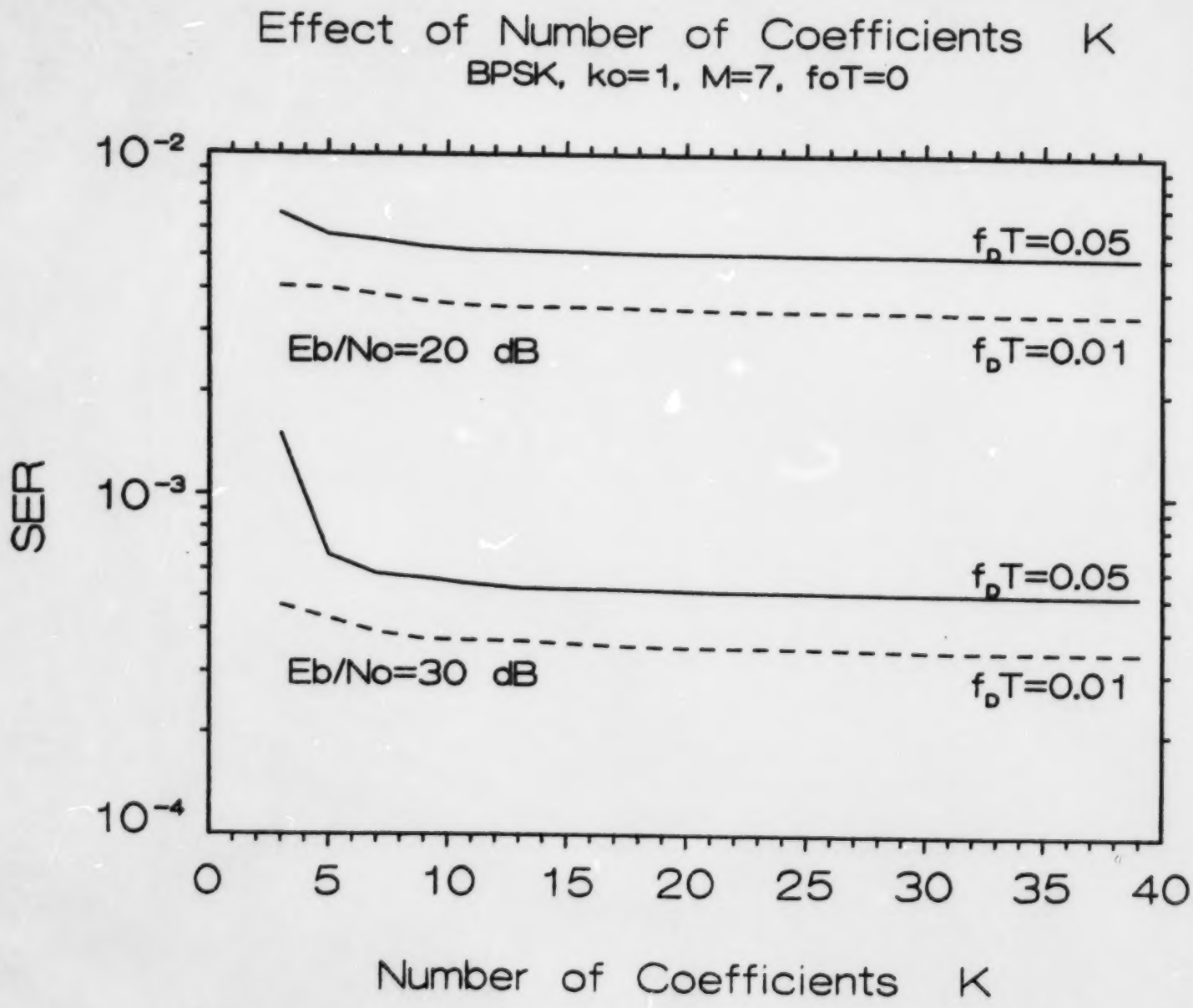

Figure 4: Effect of Interpolator Size on BPSK (M=7)

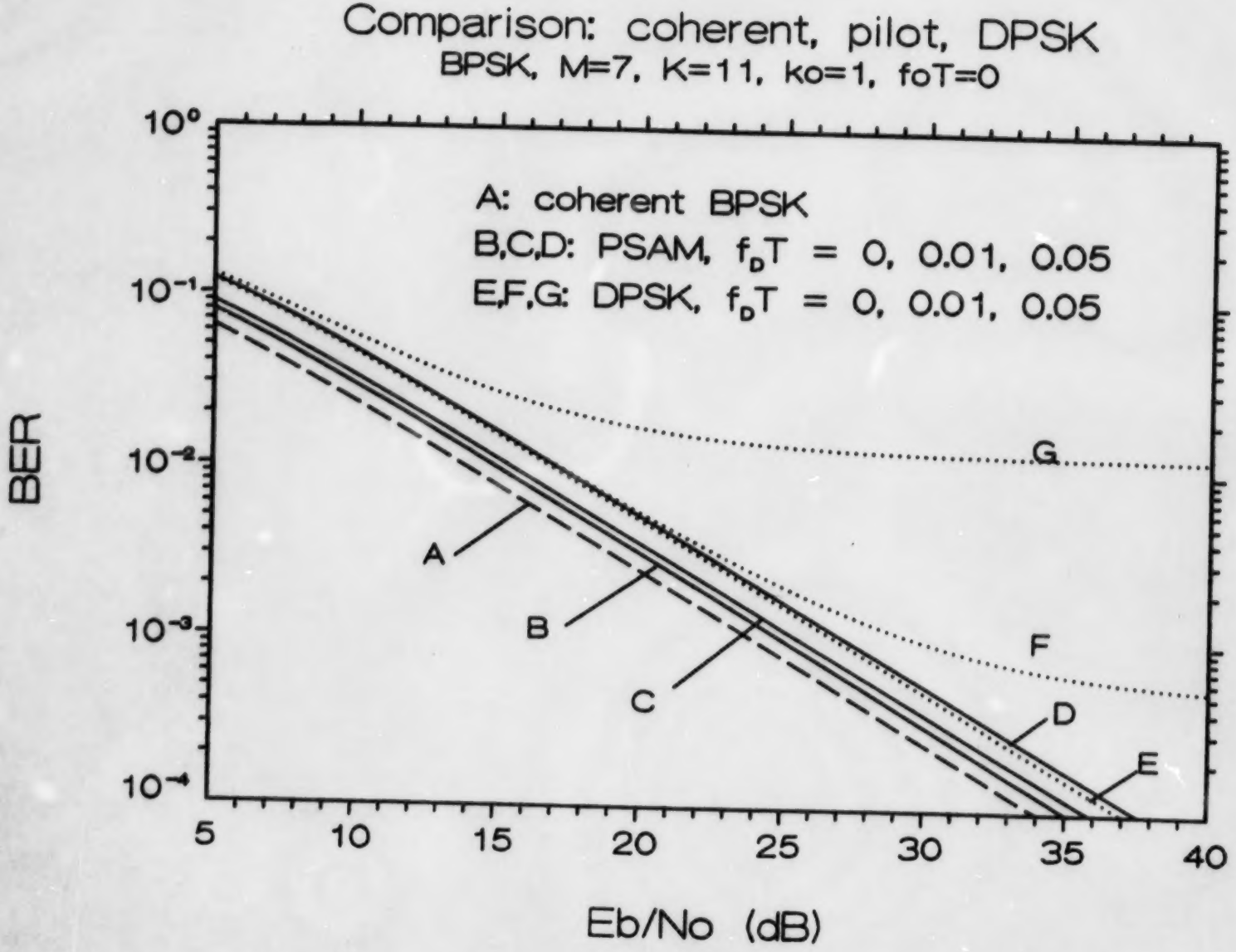

Figure 5: BER Performance of Optimized PSAM for BPSK

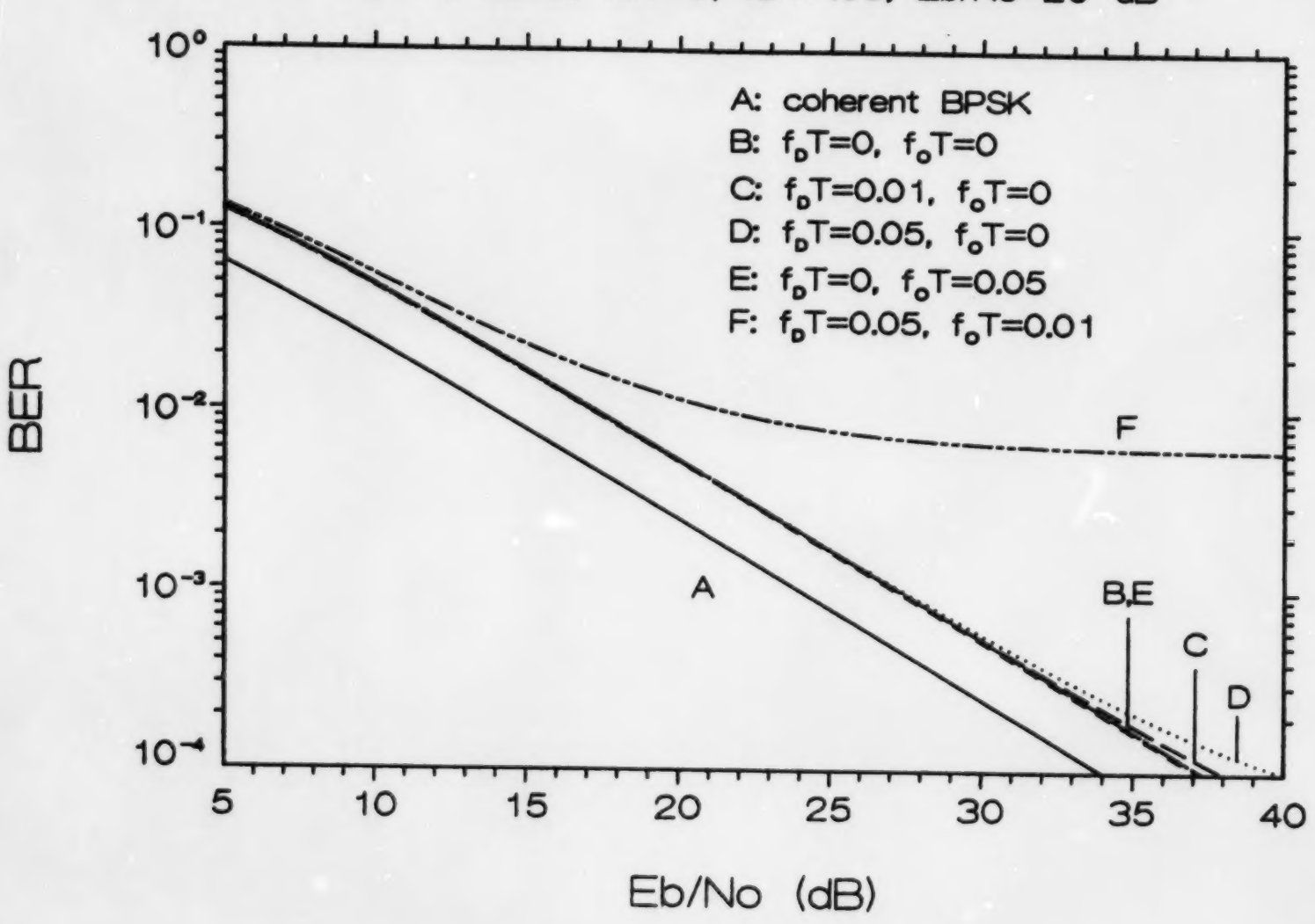

Figure 6: PSAM BPSK: Mismatched With Coefficients Optimized for γ_b=20 dB, f_oT=0, f_DT=0.05

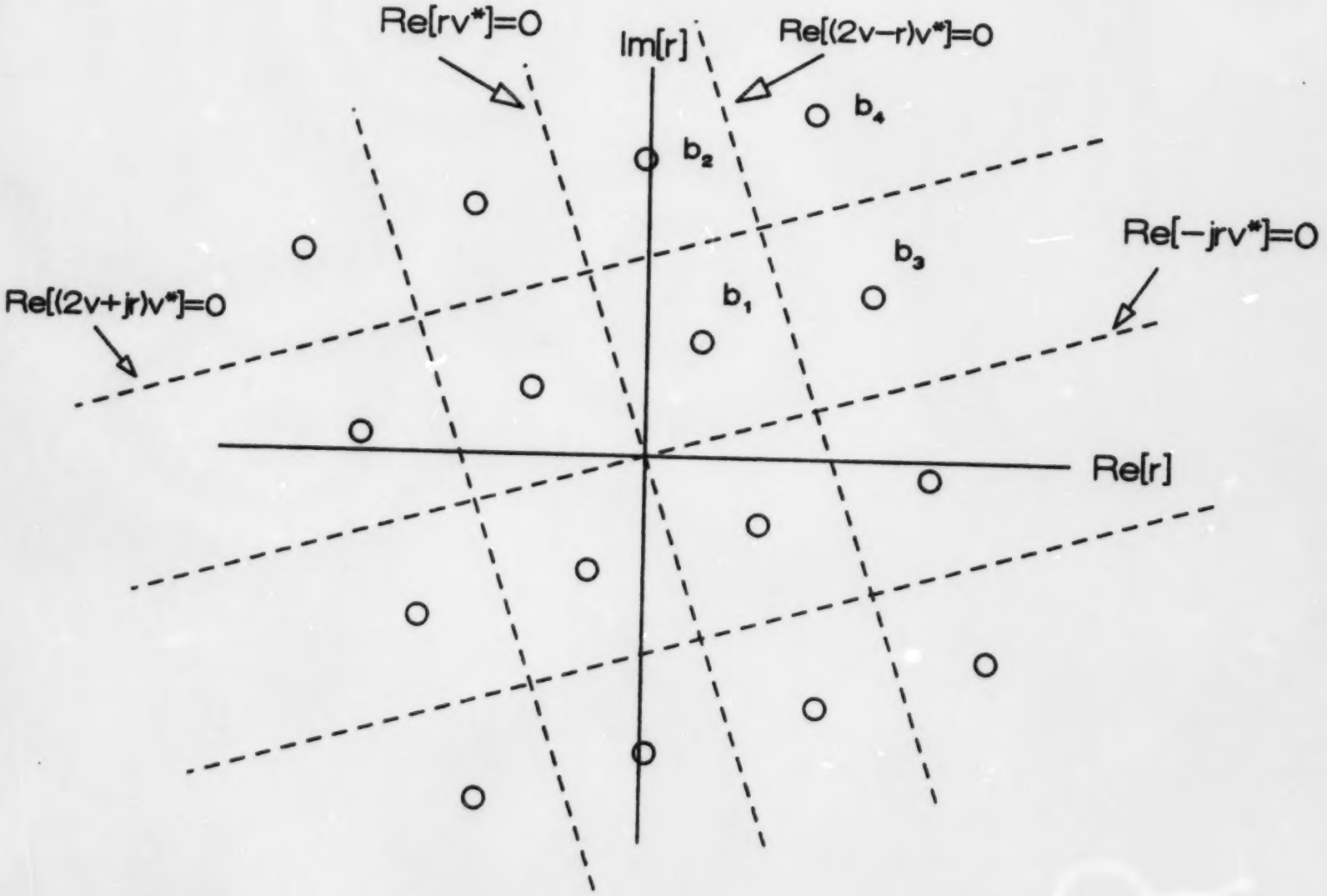

Figure 7: 16QAM Constellation and Decision Boundaries in Fading

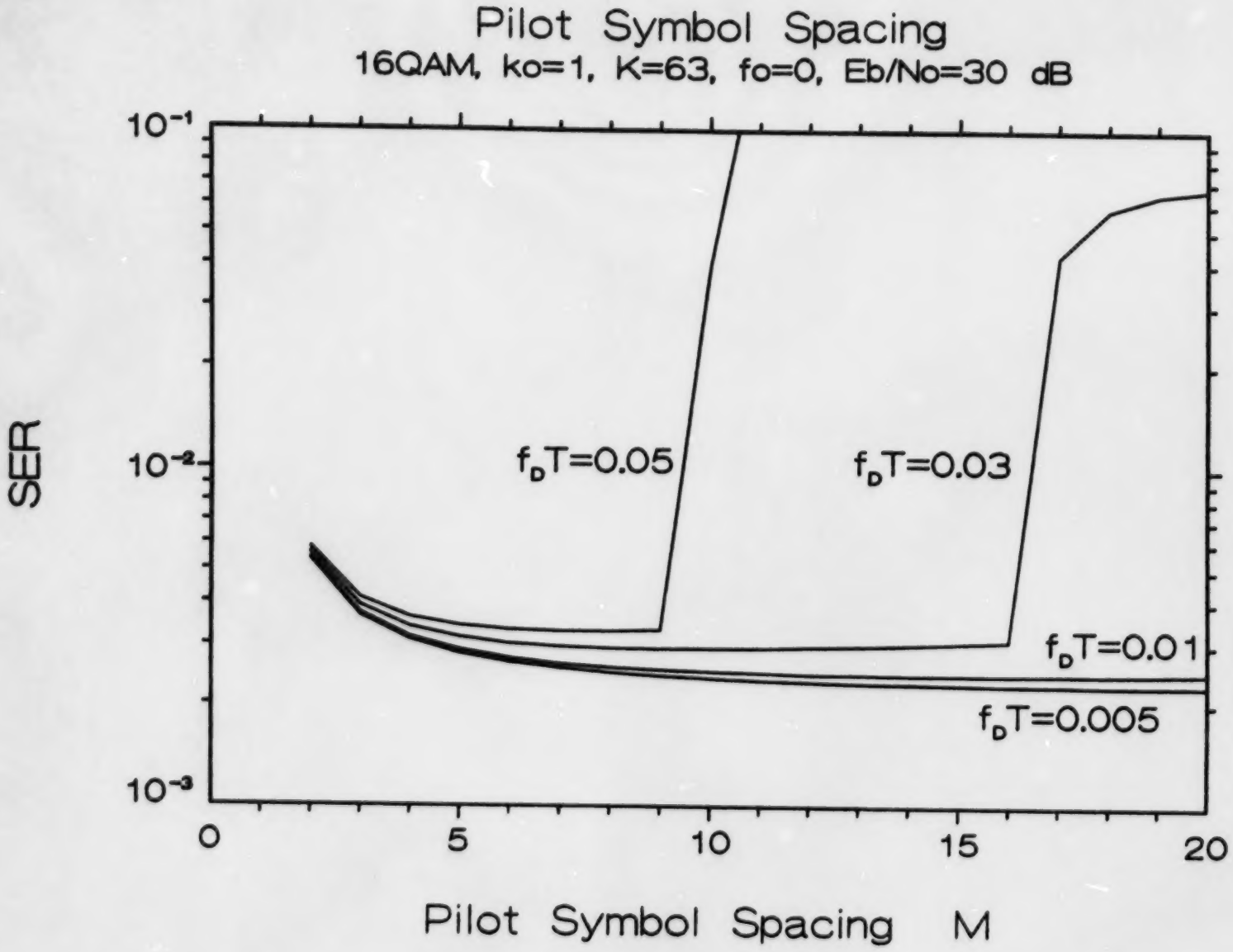

Figure 8: Effect of Frame Size on 16QAM (γ_b=30 dB, K=63)

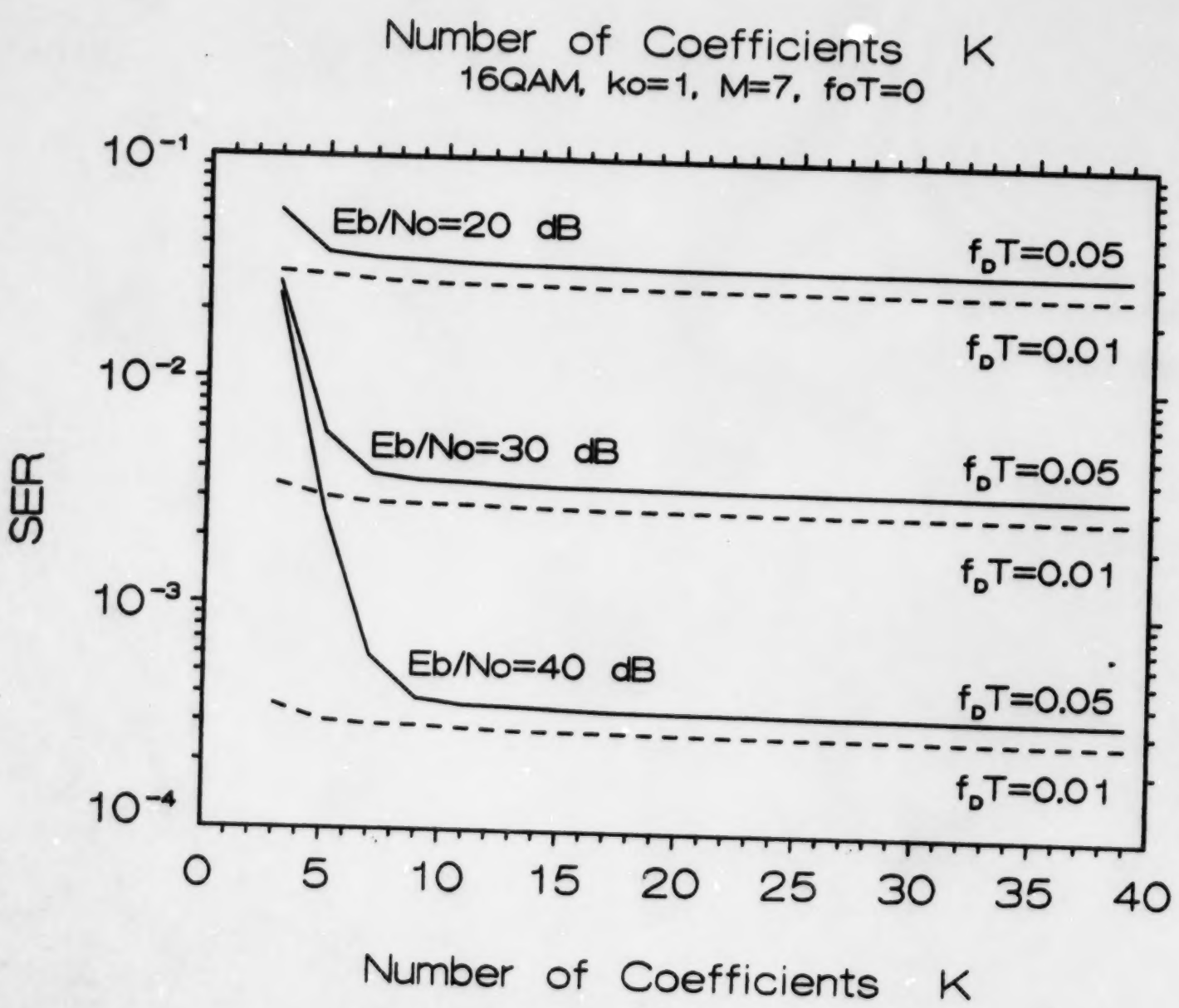

Figure 9: Effect of Interpolator Size on 16QAM (M=7)

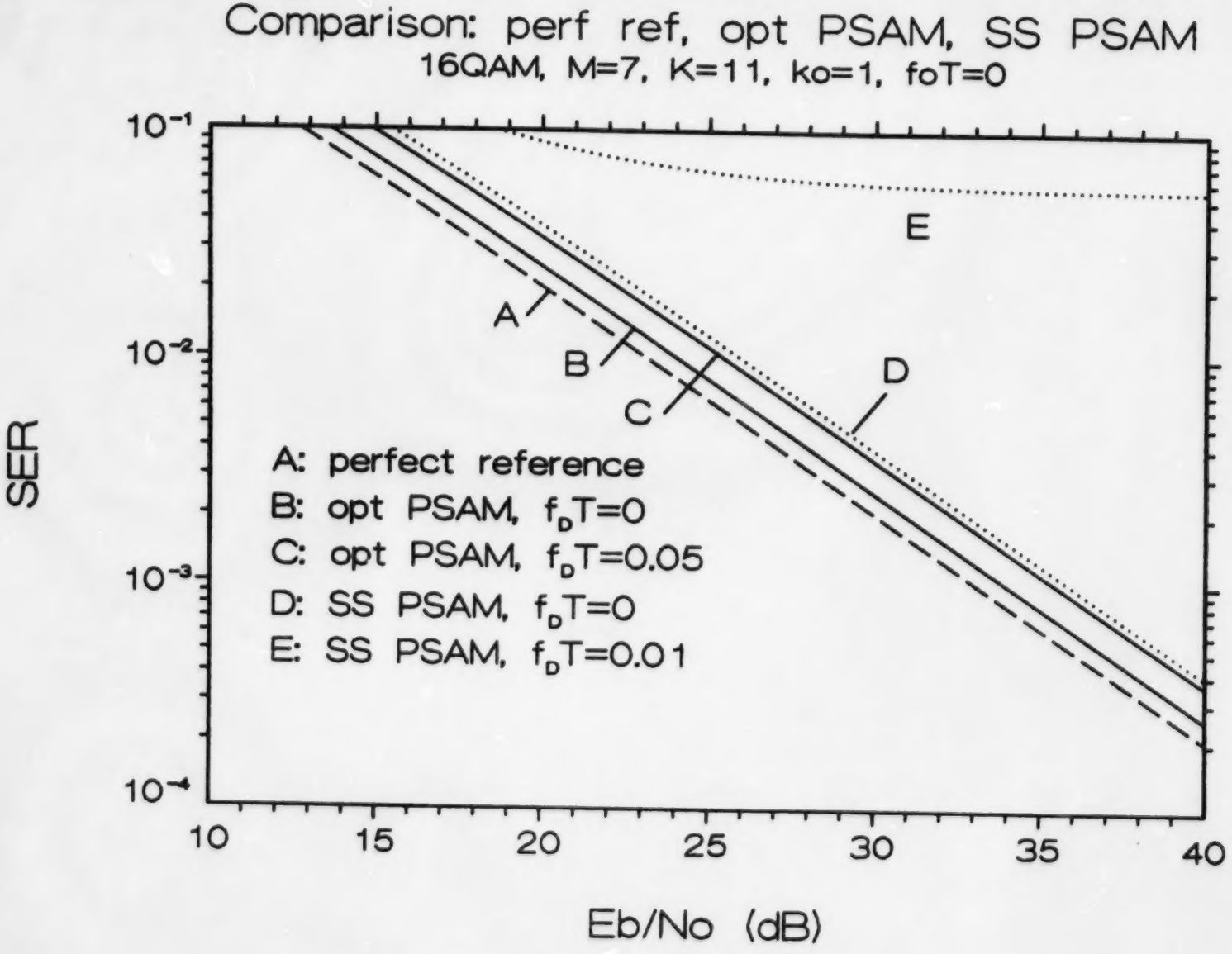

Figure 10: SER Performance of Optimized PSAM for 16QAM

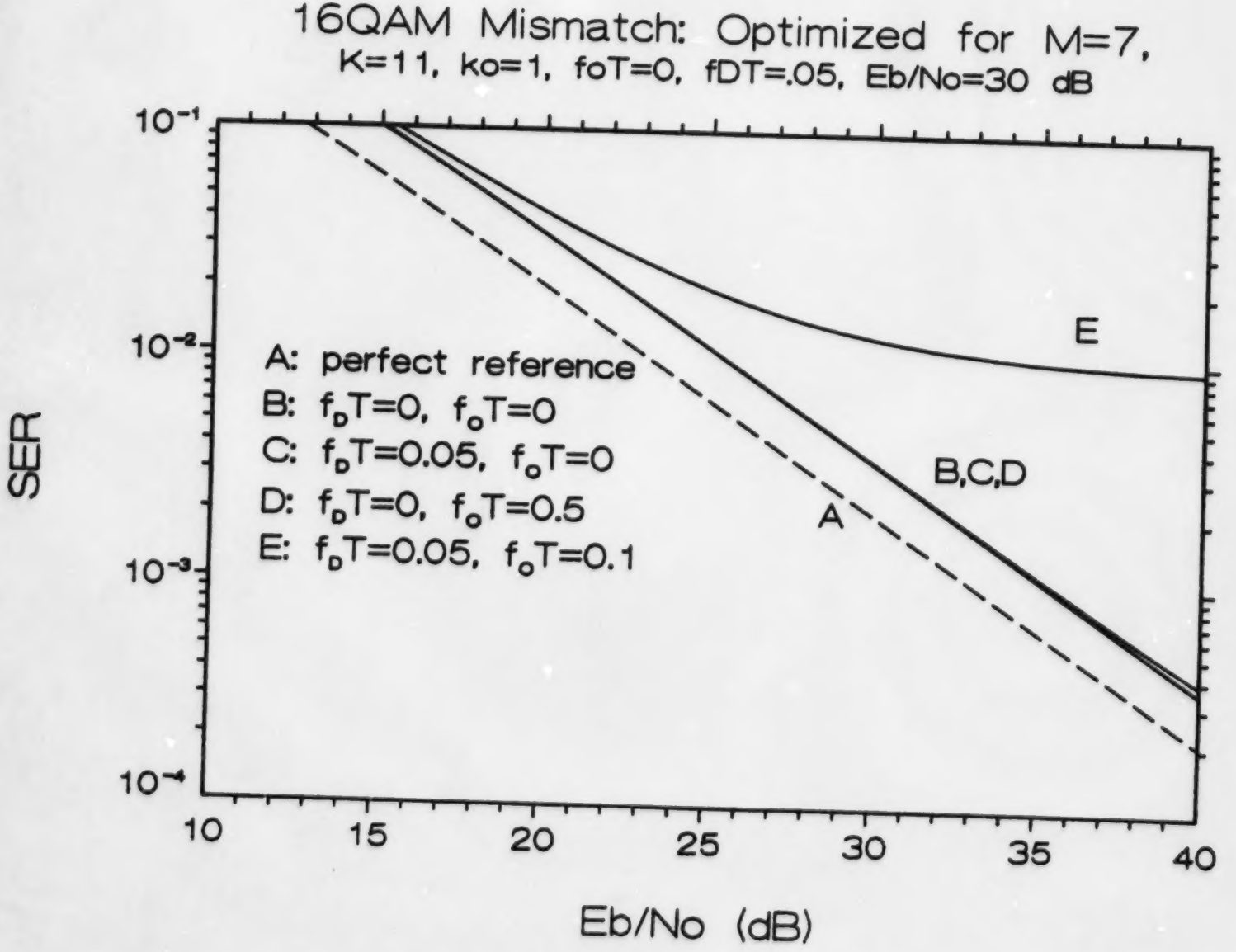

Figure 11: PSAM 16QAM: Mismatched With Coefficients Optimized for γ_b=30 dB, f_oT=0, f_DT=0.05

Centre for Systems Science

• Simon Fraser University established the **Centre for Systems Science** as a provincial centre for advanced study. The objective of CSS is twofold: coordinate and combine advanced systems research at SFU, and encourage application of research results within industry in order to further the technological development of British Columbia.

•CSS has assembled three research groups to streamline its efforts. The orientation of these groups is as follows: intelligent systems, microelectronics, and computer and communications systems. Because of shared research interests, this latter group merges with LCCR (**Laboratory for Computer and Communications Research**) for the publication of technical reports.

• CSS's three groups involve over 80 skilled faculty researchers principally from SFU's Schools of Engineering Science and Computing Science, but also draw substantially on Mathematics, Physics, Geography, Philosophy, Linguistics, Psychology, Communication, and Kinesiology.